Supplementary Information (SI) for Journal of Materials Chemistry A.
This journal is © The Royal Society of Chemistry 2026

An ultrathin carbon-shelled indium oxide catalyst for electroreduction of CO_2 to formate at ampere-level current density

Jiong-Qing Gao, Hao-Lin Zhu*, Pei-Qin Liao*, Xiao-Ming Chen

Supplementary Index

Experimental details

Materials and Measurements

All reagents and solvents in this work were commercially available and used without further purification. Piperazine and $InCl_3$ were purchased from Macklin, while 4,5-imidazoledicarboxylic acid was purchased from Aladdin. Power X-ray diffraction (PXRD) patterns were collected on a Miniflex 600 Advance diffractometer (Cu $K\alpha$). Scanning electron microscopy (SEM) images were recorded by a SU8010. Transmission electron microscope (TEM) images were recorded by a TEM (JEM-ARM200P) working at 200 kV. X-ray photoelectron spectroscopy (XPS) measurements were performed on an ESCALAB 250 instrument. Attenuated total reflection Fourier transform infrared spectroscopy (ATR-FTIR) experiments were performed on a Nicolet iS50 (Thermo Fisher) spectrometer. ^1H nuclear magnetic resonance (^1H NMR) spectroscopy measurements were performed on a Bruker AVANCE-400 MHz spectrometer.

***Operando* attenuated total reflection Fourier transform infrared spectroscopy (ATR-FTIR) measurements**

Operando ATR-FTIR spectra were recorded on a Nicolet iS50 FTIR Thermo Fisher spectrometer. Firstly, 30 μL of sample ink was coated on a glass carbon electrode (0.5 cm^2) and naturally dried to prepare the electrode, which is pressed on a germanium crystal in a special electrolytic cell by using a spiral micrometer for infrared signal capture. Then 7 mL of 0.1 M $KHCO_3$ solution was added into the cell. The data were collected at −1.1 V vs. RHE with an Ag/AgCl reference electrode and a platinum wire electrode after purging with high purity CO_2 gas for 20 min, and the FTIR spectra were recorded manually at different time in a 20-minute duration.

Density functional theory (DFT) calculations were performed by the Materials Studio 5.5 package. The structures of all intermediates in electrocatalysis were firstly optimized by $Dmol^3$ module, and the energies were obtained by calculating frequency. The generalized gradient approximation (GGA) with the Perdew-Burke-Ernzerhof (PBE) function and TS for DFT-D correction were employed to the calculation. The convergence tolerance of energy, force and displacement convergence were set as 1×10^{-5} Ha, 2×10^{-3} Ha and 5×10^{-3} Å, respectively. The core was treated using the effective core potential (ECP), and the electrons were treated by double numerical plus *d*-functions (DNP) basis set.

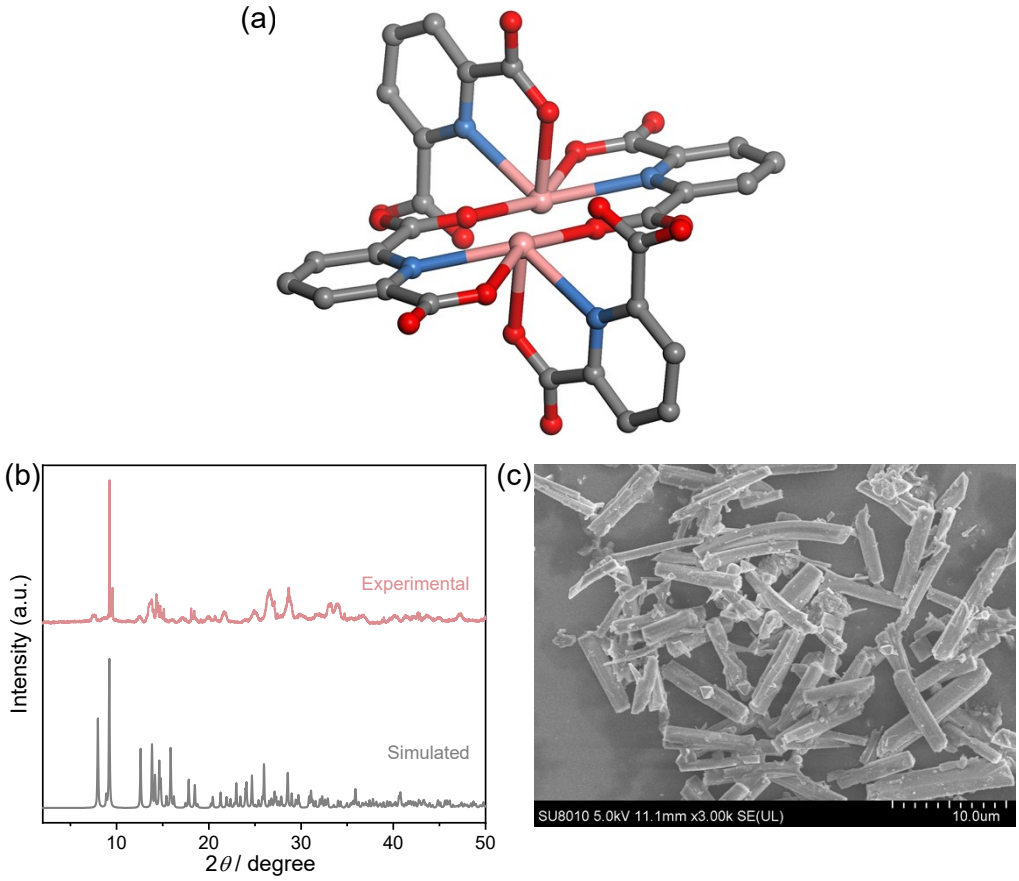

Figure S1. (a) Molecular structure, (b) PXRD patterns, and (c) SEM image of $[In_2(HIDC)_2(IDC)_2]$.

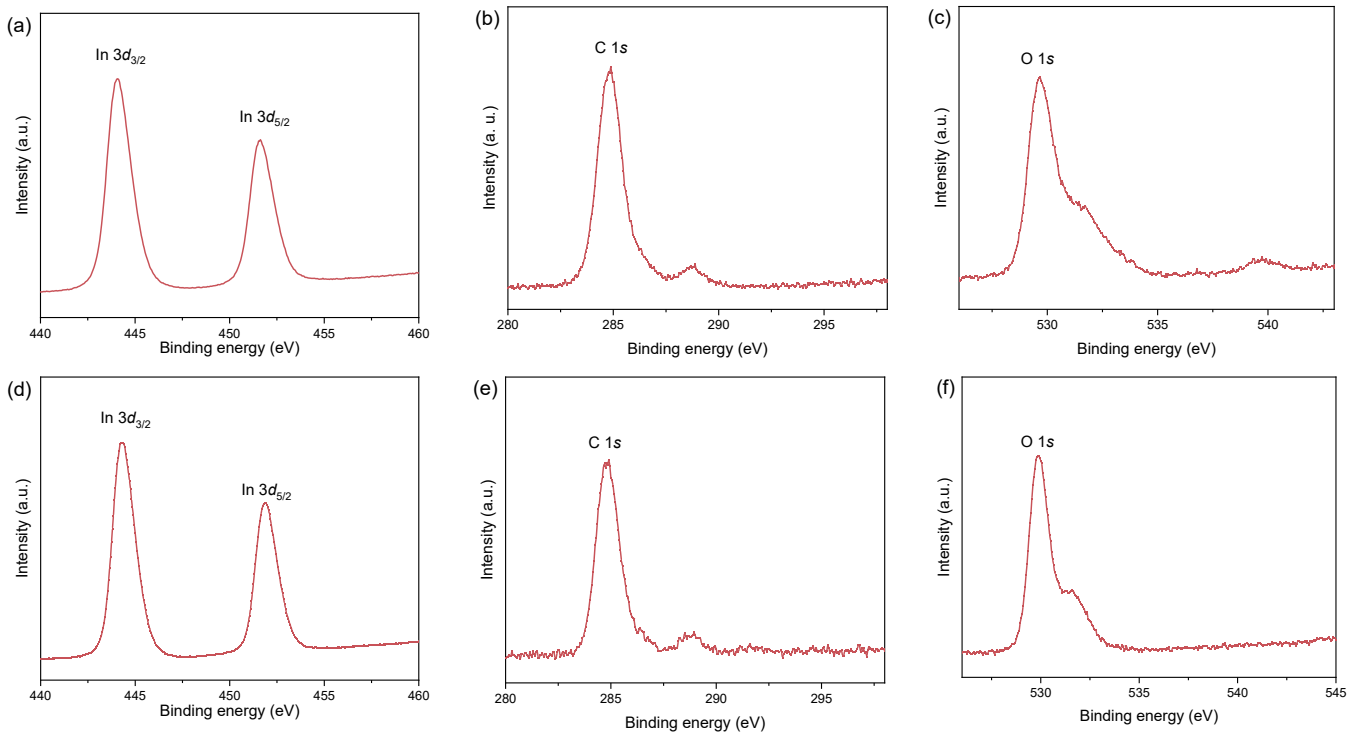

Figure S2. In 3*d* XPS spectrum of In_2O_3@C (a-c) before and (d-e) after electrolysis.

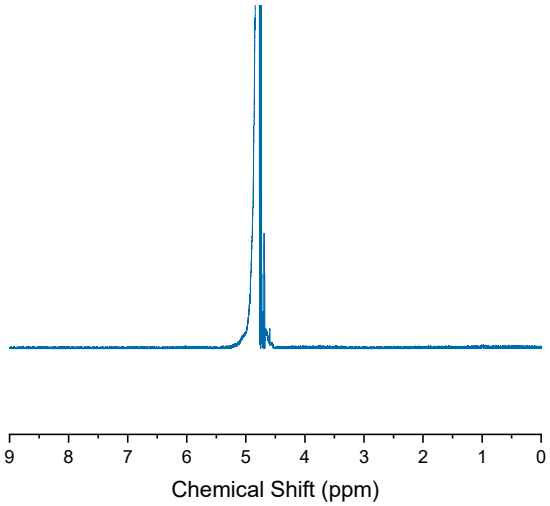

Figure S3. ^{1}H NMR of hydrochloric acid after as-synthesized In_2O_3@C immersion.

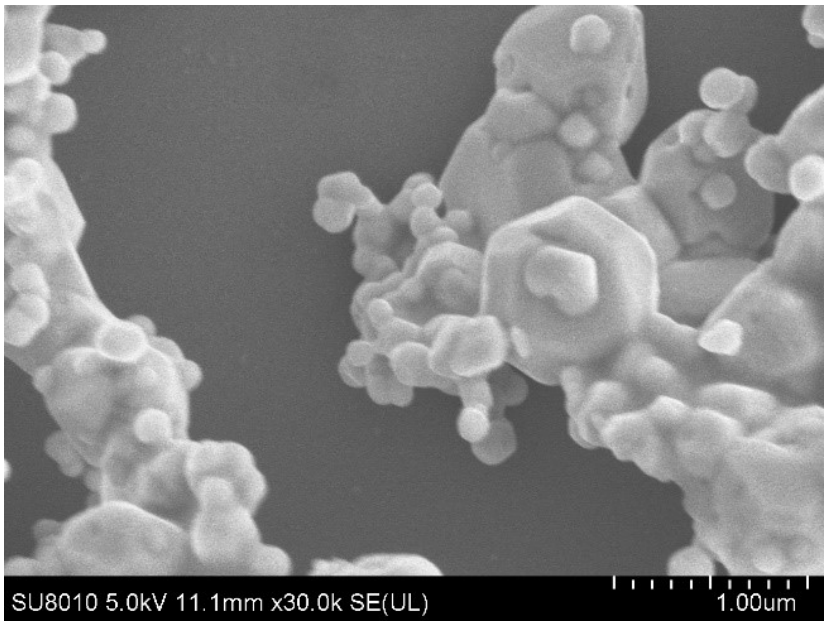

Figure S4. SEM image of In_2O_3@C.

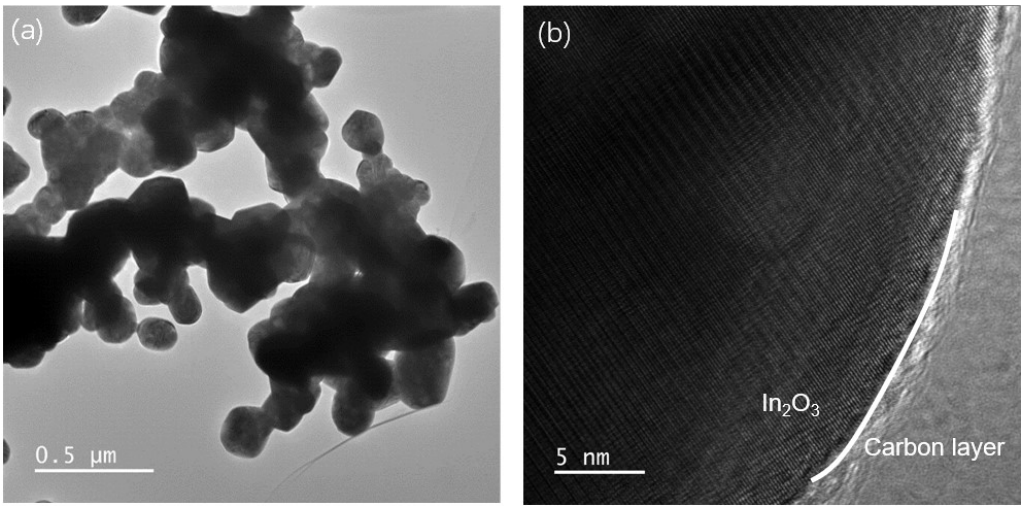

Figure S5. TEM image of In_2O_3@C before(a) and after(b) electrolysis.

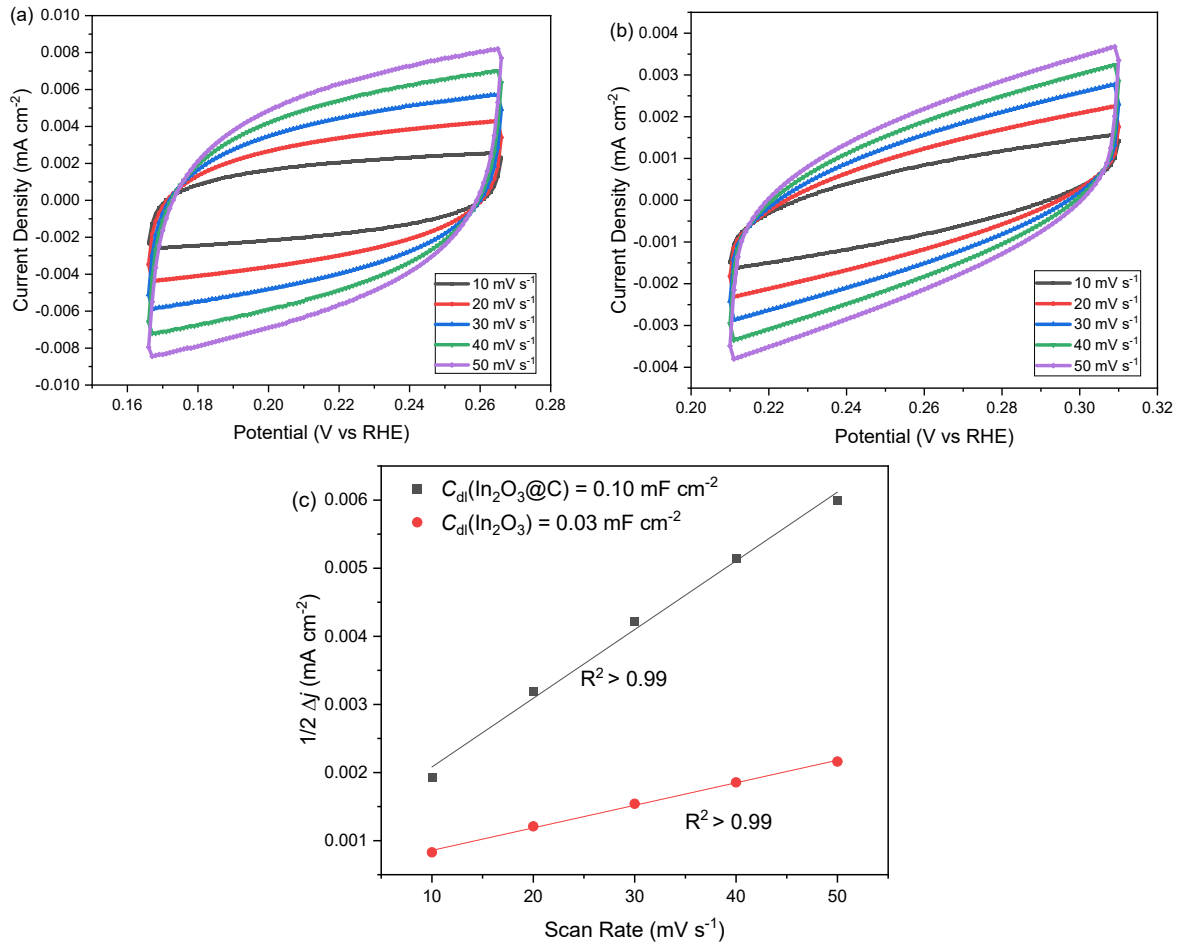

Figure S6 Cyclic Voltammetry (CV) curves of (a) In_2O_3@C and (b) In_2O_3, respectively. Double-layer capacitance(c) obtained by linear fitting of CV.

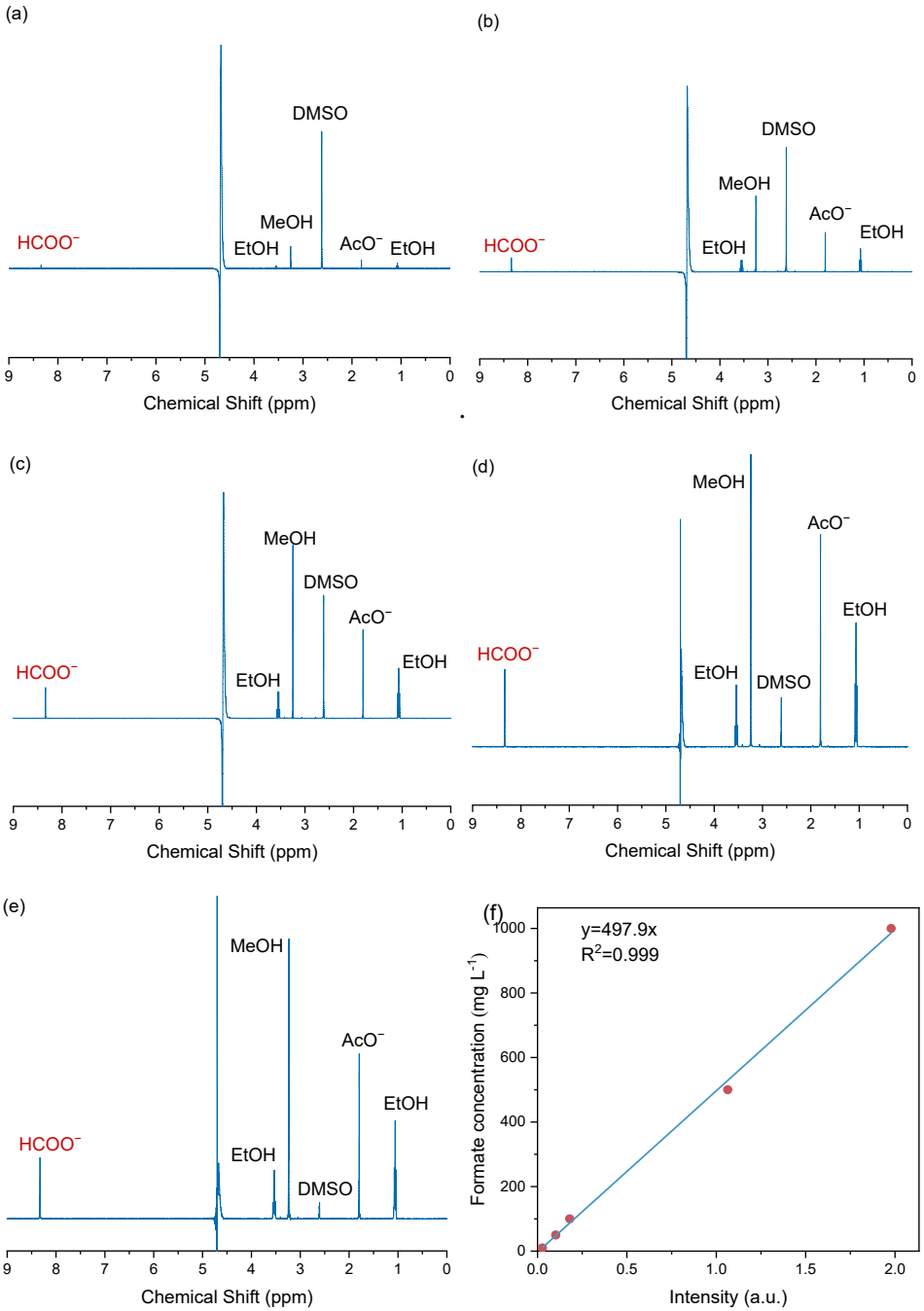

Figure S7. ^{1}H NMR spectra of formate standard solutions with different concentrations of (a) 10, (b) 50, (c) 100, and (d) 500 (e) 1000 mg L^{-1}. (f) Calibration curve of standard solutions for the determination of formate.

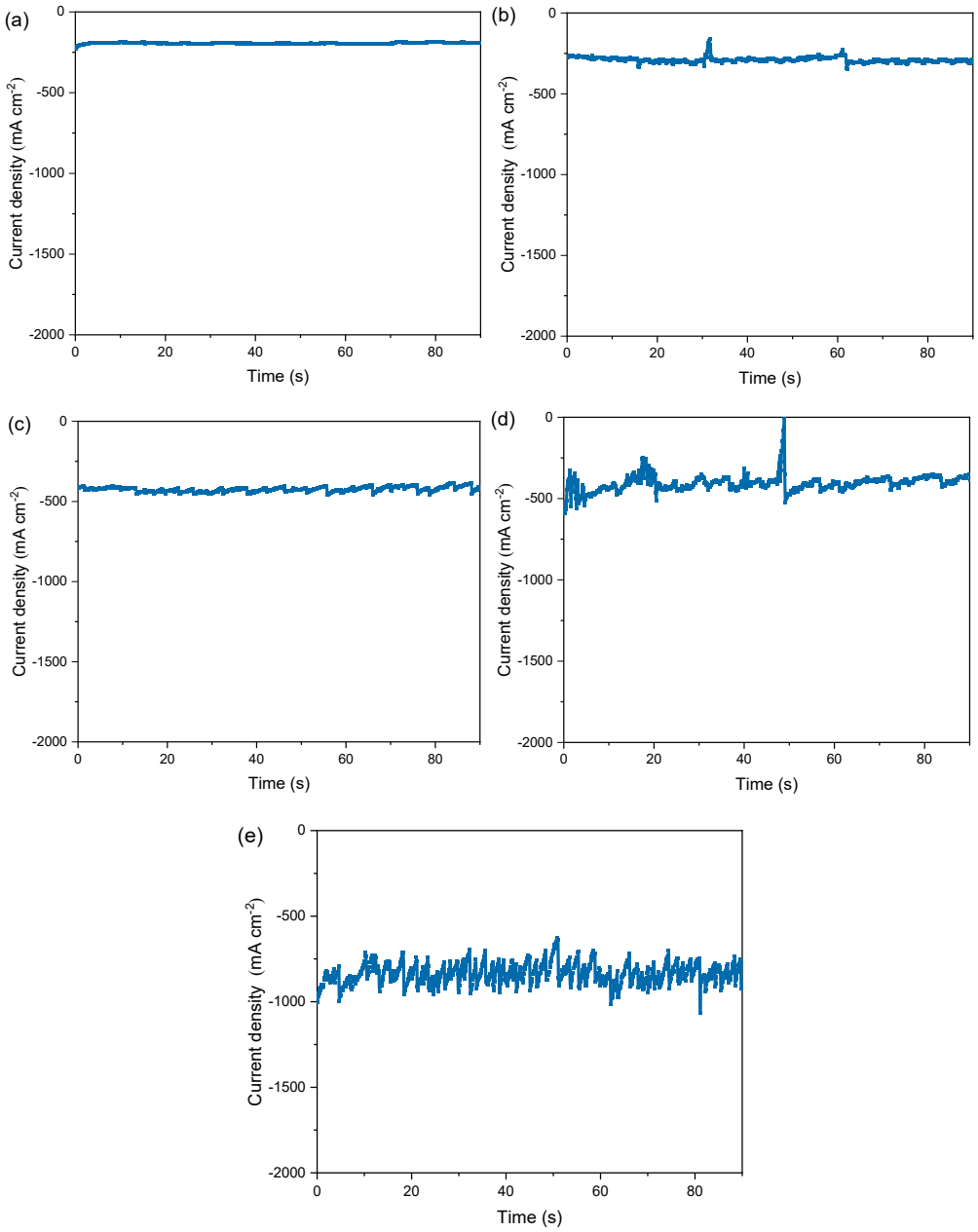

Figure S8. Chronopotentiometry test of In_2O_3@C at the potentials of (a) −1.1 V vs. RHE, (b) −1.3 V vs. RHE, (c) −1.5 V vs. RHE, (d) −1.7 V vs. RHE (e) −1.9 V vs. RHE.

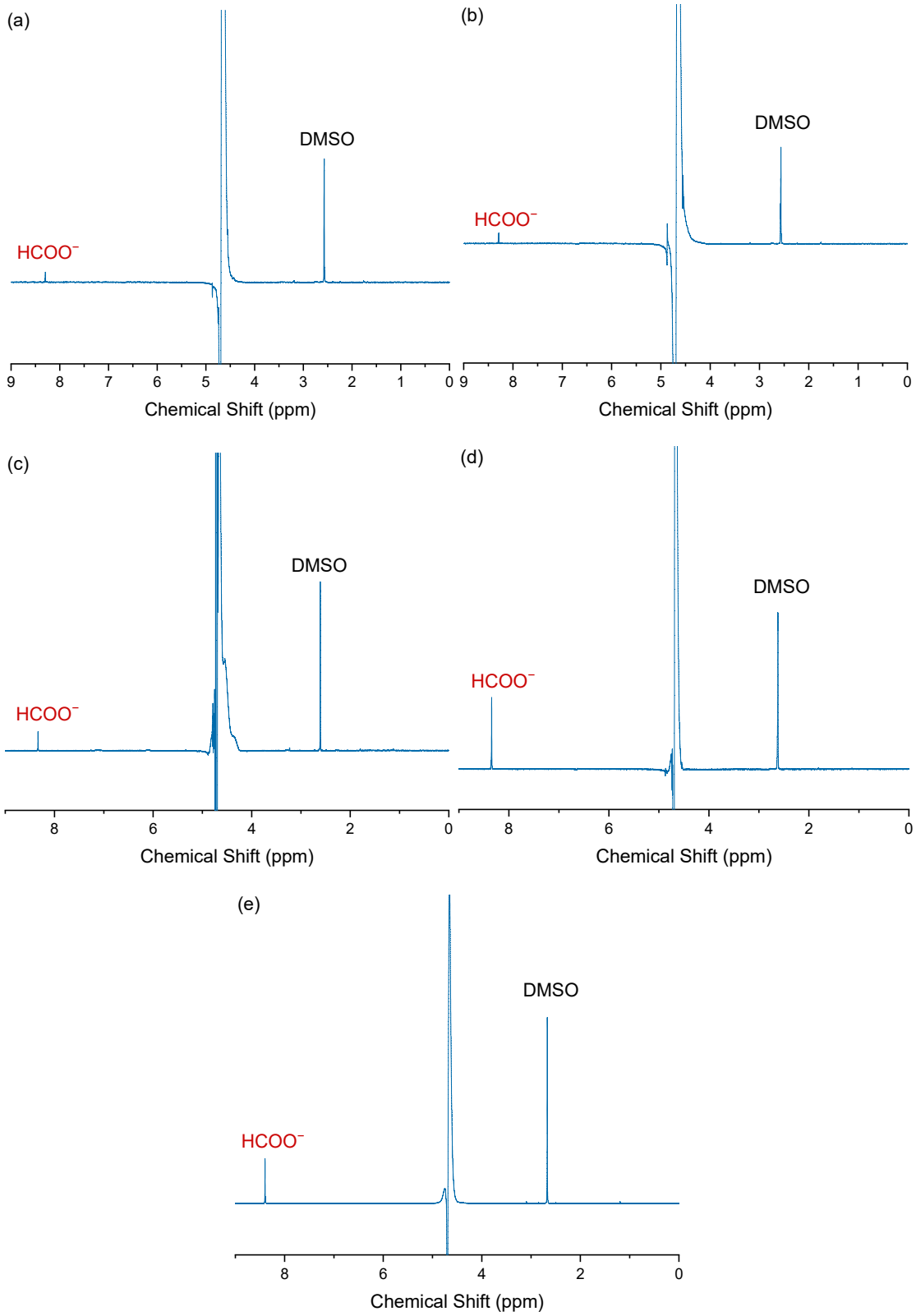

Figure S9. ^{1}H NMR spectra of liquid products for eCO_2RR by In_2O_3@C catalyst at the potentials of (a) −1.1 V vs. RHE, (b) −1.3 V vs. RHE, (c) −1.5 V vs. RHE, (d) −1.7 V vs. RHE (e) −1.9 V vs. RHE.

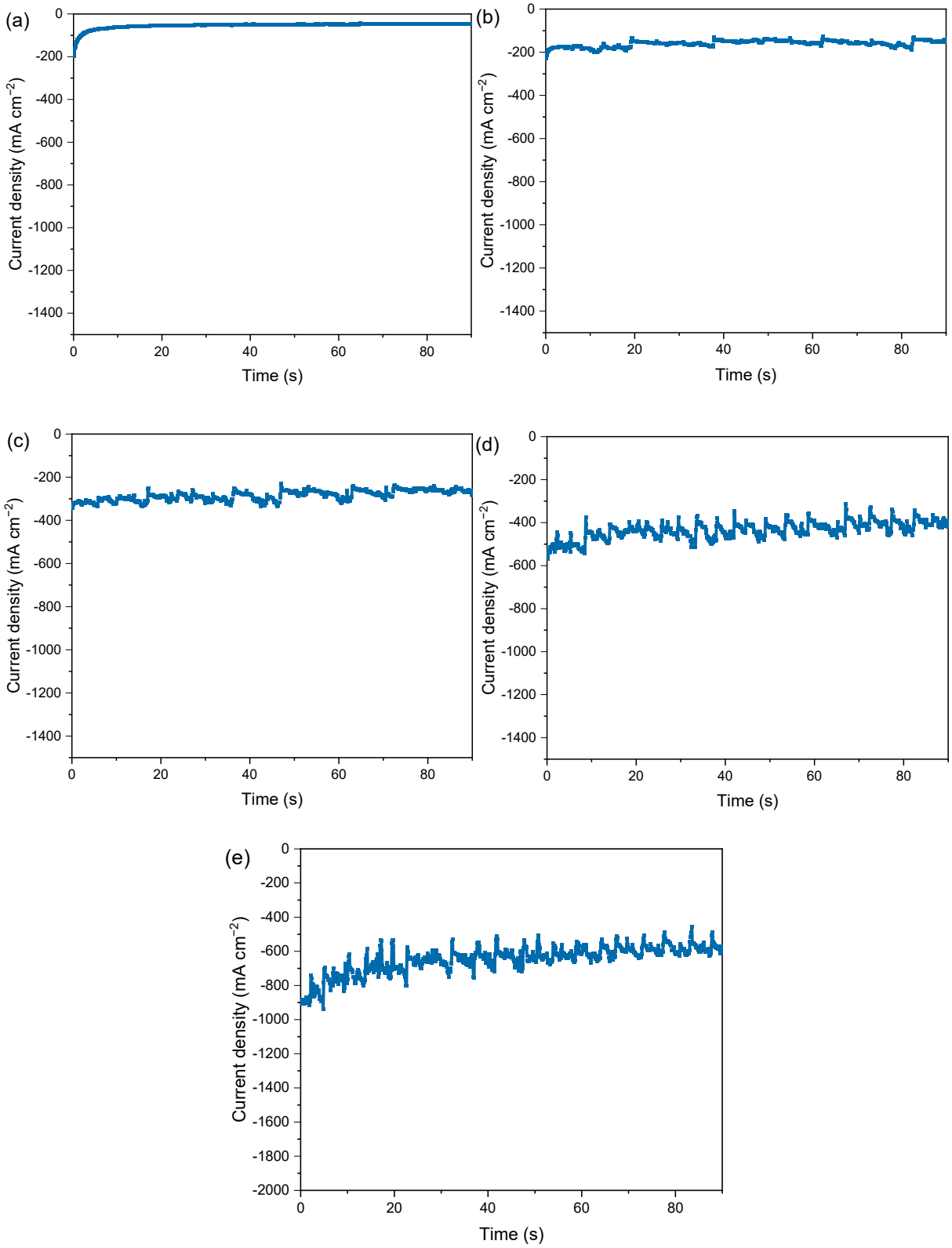

Figure S10. Chronopotentiometry test of commercial In_2O_3 at the potentials of (a) −1.1 V vs. RHE, (b) −1.3 V vs. RHE, (c) −1.5 V vs. RHE, (d) −1.7 V vs. RHE (e) −1.9 V vs. RHE.

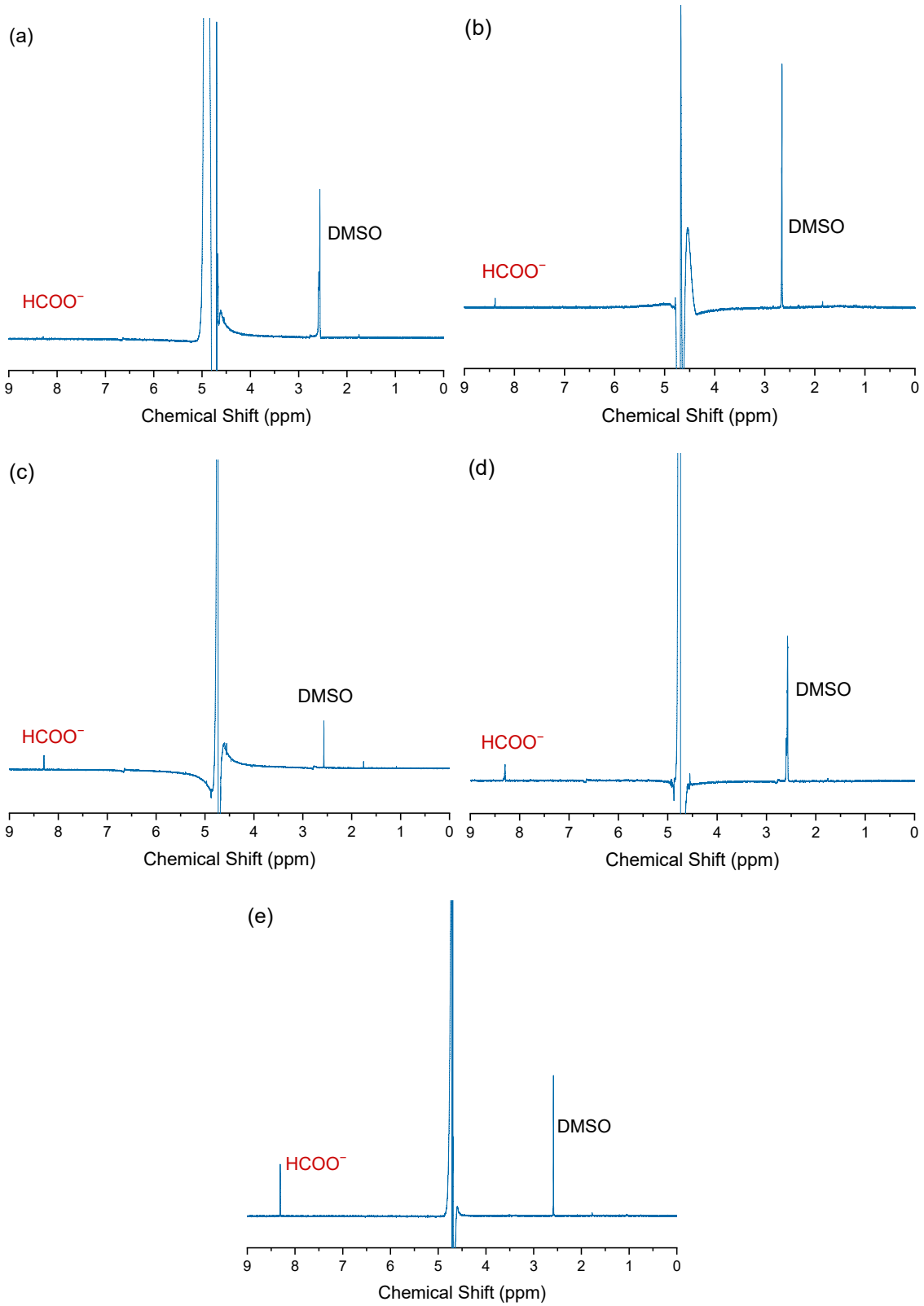

Figure S11. ^{1}H NMR spectra of liquid products for eCO_2RR by commercial In_2O_3 at the potentials of (a) −1.1 V vs. RHE, (b) −1.3 V vs. RHE, (c) −1.5 V vs. RHE, (d) −1.7 V vs. RHE (e) −1.9 V vs. RHE.

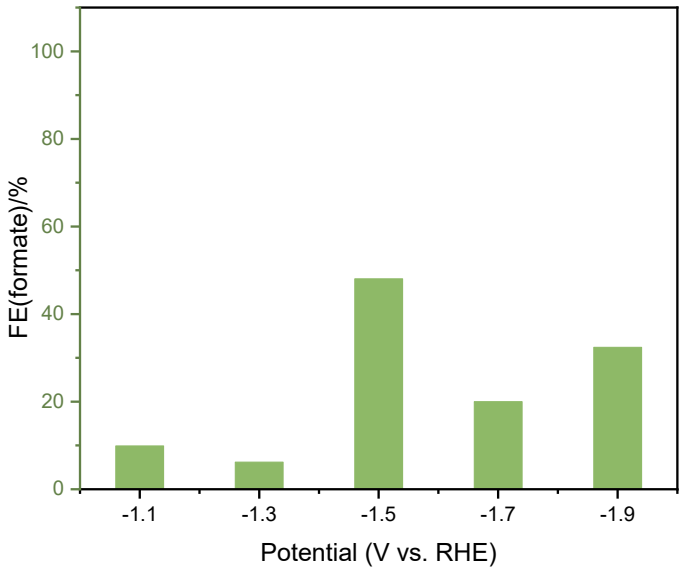

Figure S12. FE(formate) of commercial In_2O_3.

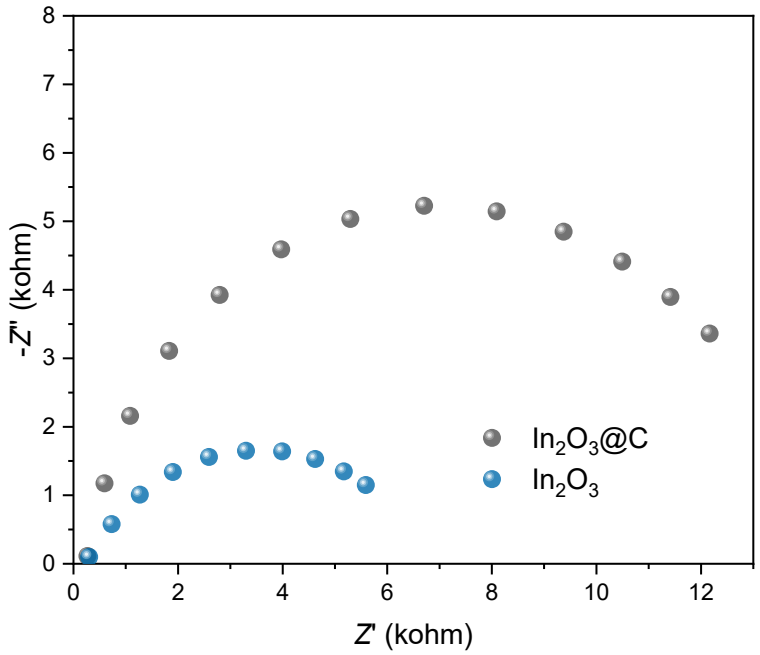

Figure S13 EIS spectra of In_2O_3 and In_2O_3@C catalysts.

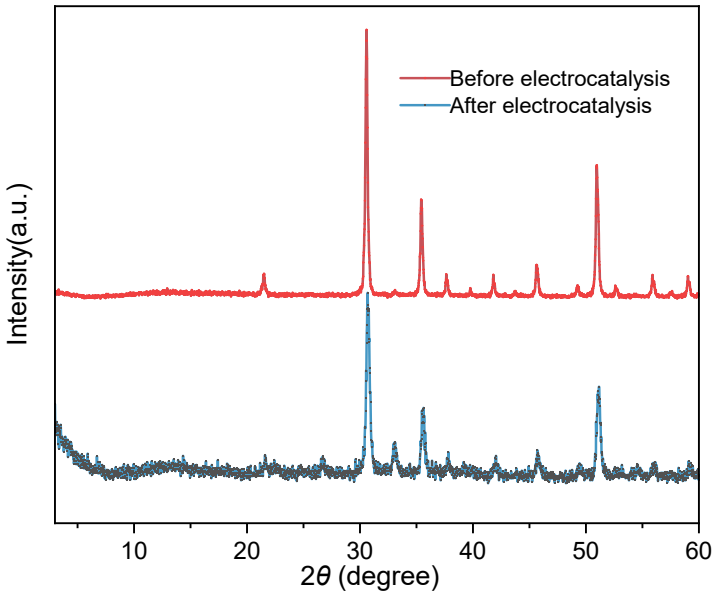

Figure S14. PXRD patterns of In_2O_3@C before and after electrocatalysis.

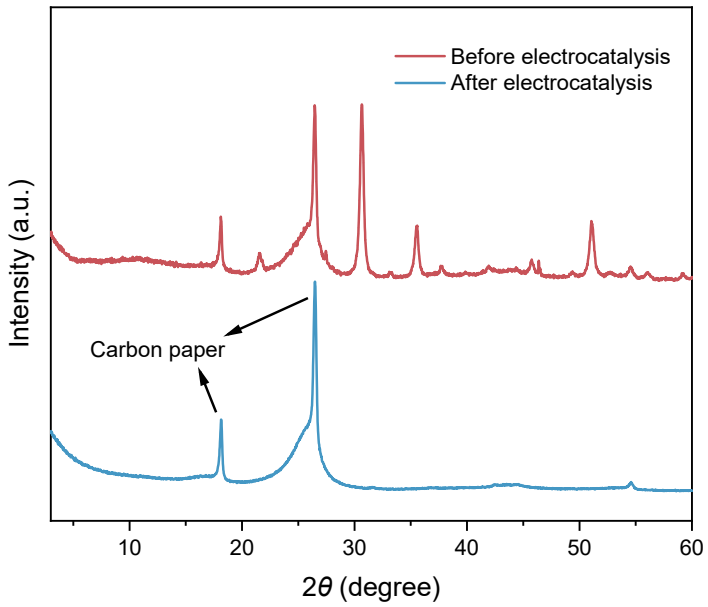

Figure S15. PXRD patterns of carbon paper loaded with commercial In_2O_3 before and after electrocatalysis. Note that most of In_2O_3 powder dissolved in 1 M KOH aqueous solution, no catalyst solid can be collected after electrolysis. Therefore, the gas diffusion electrodes before and after electrolysis were directly used for the collection of PXRD patterns.

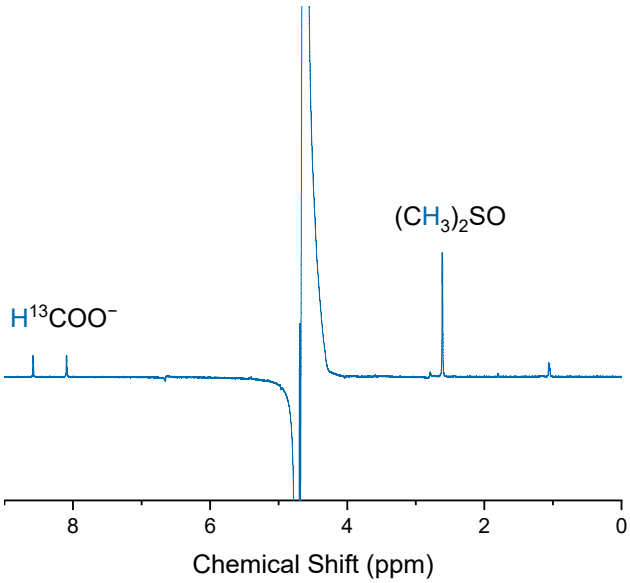

Figure S16. ^{1}H NMR spectra of liquid products for eCO_2RR by In_2O_3@C catalyst under $^{13}CO_2$.

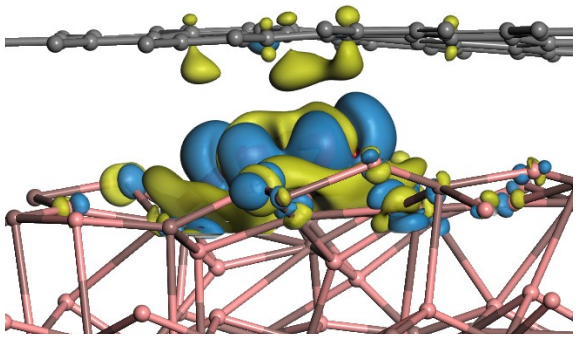

Figure S17. Differential charge density mapping of the *OCHO intermediate.

Table S1. ICP-AES results of electrolyte.

Catholyte	Concentration of In (mg L^{-1})
before electrolysis	−0.025
after electrolysis	−0.029

The negative value refers to that no indium detected.

Table S2. Performance comparison of electrocatalytic formate synthesis.

Catalyst	Electrolyte	Potential (V vs. RHE)	FE(fomate) (%)	Current density (mA cm^{-2})	Stability (h)	Ref.
In_2O_3@C	1 M KOH	−1.9	85	833	110	This work
In_2O_3/Bi_2O_3	1 M KOH	−0.7	93	3	30	[1]
In/In_2O_3	1 M KOH	−0.6	94	100	13	[2]
In_2O_3/CZ-r	1 M KOH	−1.2	100	80	60	[3]
In_2O_3-C	1 M KOH	−1.2	85	200	15	[4]
Ni-In_2O_3@C NFs	1 M KOH	−0.8	86	350	55	[5]
In_2O_3@C	1 M KOH	−1.1	94	70	9	[6]
In_2O_3	1 M KOH	−0.7	85	90	18	[7]
In_2O_3	0.1M $KHCO_3$	-1.3	85	18	80	[8]

References

1. Y. Wang, H. Jiang, Z. Guo, H. Ma, S. Wang, H. Wang, S. Song, J. Zhang, Y. Yin, H. Wu, Z. Jiang and M. D. Guiver, *Energy Environ. Sci.*, 2023, **16**, 53-75.
2. B. Wulan, X. Cao, D. Tan, J. Ma and J. Zhang, *Adv. Funct. Mater.*, 2022, **33**, 2209114.
3. R. Qi, M. Liang, Z. Miao, H. Xu, Y. Fan, J. Mu, W. Feng, L. Diao, J. Zhou, X. Li and T. Ma, *Adv. Funct. Mater.*, 2025, DOI: 10.1002/adfm.202510948, e10948.
4. W. Wang, X. Wang, Z. Ma, Y. Wang, Z. Yang, J. Zhu, L. Lv, H. Ning, N. Tsubaki and M. Wu, *ACS Catal.*, 2022, **13**, 796-802.
5. Z. Chen, G. Yu, B. Li, X. Zhang, M. Jiao, N. Wang, X. Zhang and L. Liu, *ACS Catal.*, 2021, **11**, 14596-14604.
6. Z. Wang, Y. Zhou, D. Liu, R. Qi, C. Xia, M. Li, B. You and B. Y. Xia, *Angew. Chem. Int. Ed.*, 2022, **61**, e202200552.
7. Y. Li, Z. Xu, Q. Guo, Q. Li and R. Liu, *J. Energy Chem.*, 2025, **101**, 474-484.
8. Q. Cheng, M. Huang, L. Xiao, S. Mou, X. Zhao, Y. Xie, G. Jiang, X. Jiang and F. Dong, *ACS Catal.*, 2023, **13**, 4021-4029.